PtdIns(3,4,5)P_3-dependent Rac exchanger 1 (P-Rex1) promotes mammary tumor initiation and metastasis

Nuthasuda Srijakotre[a,1], Heng-Jia Liu[a,1,2], Max Nobis[b], Joey Man[a], Hon Yan Kelvin Yip[a], Antonella Papa[a], Helen E. Abud[c], Kurt I. Anderson[d,e], Heidi C. E. Welch[f], Tony Tiganis[a,g], Paul Timpson[b], Catriona A. McLean[h], Lisa M. Ooms[a,3], and Christina A. Mitchell[a,3,4]

[a]Cancer Program, Monash Biomedicine Discovery Institute and Department of Biochemistry and Molecular Biology, Monash University, Clayton, VIC 3800, Australia; [b]Garvan Institute of Medical Research, Faculty of Medicine, St Vincent's Clinical School, University of New South Wales (UNSW) Sydney, Darlinghurst, NSW 2010, Australia; [c]Development and Stem Cells Program, Monash Biomedicine Discovery Institute and Department of Anatomy and Developmental Biology, Monash University, Clayton, VIC 3800, Australia; [d]Tumour Cell Migration, Cancer Research UK Beatson Institute, G611BD Glasgow, United Kingdom; [e]Crick Advanced Light Microscopy, Francis Crick Institute, NW11AT London, United Kingdom; [f]Signalling Programme, Babraham Institute, CB22 3AT Cambridge, United Kingdom; [g]Peter MacCallum Cancer Centre, Melbourne, VIC 3000, Australia; and [h]Department of Anatomical Pathology, Alfred Hospital, Prahran, VIC 3181, Australia

Edited by Joan S. Brugge, Harvard Medical School, Boston, MA, and approved September 2, 2020 (received for review April 7, 2020)

The Rac-GEF, P-Rex1, activates Rac1 signaling downstream of G protein-coupled receptors and PI3K. Increased P-Rex1 expression promotes melanoma progression; however, its role in breast cancer is complex, with differing reports of the effect of its expression on disease outcome. To address this we analyzed human databases, undertook gene array expression analysis, and generated unique murine models of P-Rex1 gain or loss of function. Analysis of *PREX1* mRNA expression in breast cancer cDNA arrays and a METABRIC cohort revealed that higher *PREX1* mRNA in ER^{+ve}/luminal tumors was associated with poor outcome in luminal B cancers. *Prex1* deletion in MMTV-*neu* or MMTV-*PyMT* mice reduced Rac1 activation in vivo and improved survival. High level MMTV-driven transgenic *PREX1* expression resulted in apicobasal polarity defects and increased mammary epithelial cell proliferation associated with hyperplasia and development of de novo mammary tumors. MMTV-*PREX1* expression in MMTV-*neu* mice increased tumor initiation and enhanced metastasis in vivo, but had no effect on primary tumor growth. Pharmacological inhibition of Rac1 or MEK1/2 reduced P-Rex1-driven tumoroid formation and cell invasion. Therefore, P-Rex1 can act as an oncogene and cooperate with HER2/neu to enhance breast cancer initiation and metastasis, despite having no effect on primary tumor growth.

breast cancer | transgenic mouse | guanine nucleotide exchange factor (GEF) | metastasis | cell polarity

Breast cancer is the most common malignancy affecting women worldwide and its incidence is increasing. Breast cancer development is associated with loss of cell growth control and disrupted tissue organization (1). Despite many recent diagnostic and treatment advances, relapse occurs in 20 to 30% of breast cancers, and metastasis is still a challenging condition with limited treatment options.

Multiple protein complexes and signaling pathways cooperate to establish and maintain cell polarity that when disrupted contribute to both cancer initiation and metastasis. The Rho GTPases regulate epithelial cell adhesion and polarity, migration, membrane traffic, and the cell division cycle (2, 3). Ras-related C3 botulinum toxin substrate 1 (Rac1), a member of the Rho family of GTPases, plays important roles in cell migration and survival (4). Rac1 contributes to the maintenance of epithelial cell apicobasolateral polarity and its modulators (GEFs/GAPs) are implicated in cancer development, invasion, and metastasis (4, 5). P-Rex1 is a Rac-GEF that contains an N-terminal DH-PH tandem domain, a centralized pair of DEP and PDZ domains, and an inactive C-terminal inositol polyphosphate 4-phosphatase (IP4P) domain (6, 7). P-Rex1 Rac-GEF activity is synergistically activated by the phosphoinositide 3-kinase (PI3K) product PtdIns(3,4,5)P_3, downstream of receptor tyrosine kinases (RTKs), and by the βγ subunit of activated heterotrimeric G proteins, following G protein-coupled receptor (GPCR) activation (8). P-Rex1 serves as an integration point between RTKs such as the HER2 (also known as ErbB2/neu) receptor and GPCR (7, 9, 10).

There are conflicting reports regarding P-Rex1 expression in breast cancer, the impact of its expression on long-term outcome, and its role in breast cancer biology. P-Rex1 expression is low/negligible in normal human mammary lobules and ducts (10, 11), but P-Rex1 mRNA and protein are frequently overexpressed in up to 50% of primary breast cancers (10–12). Some studies have shown higher P-Rex1 mRNA and protein expression in ER-positive luminal breast cancers (10, 12–14) and the *PREX1* gene was recently identified as a primary target of ERα (15). Dillon et al. also suggested a modest negative correlation between P-Rex1 protein expression and HER2 amplification (13). High P-Rex1 protein expression was associated with decreased disease-free survival in one study, although the sample size of this report was small ($n = 32$ low P-Rex1-expressing and $n = 4$ high P-Rex1-expressing tumors) (11). Conversely, another

Significance

Breast cancer is the most common cancer in women and metastasis remains the leading cause of death. P-Rex1, a guanine nucleotide exchange factor, positively regulates Rac1-mediated oncogenic signaling. P-Rex1 is overexpressed in a subset of human breast cancers; however, little is known of its function in vivo. Here we show P-Rex1 regulates Rac1 activation in vivo in the mammary gland. Increased P-Rex1 expression enhances mammary epithelial cell proliferation and is causally associated with tumor initiation. In murine models, P-Rex1 cooperates with the neu oncogene to increase mammary tumor incidence and metastasis but not primary tumor growth. Our studies suggest that inhibiting the P-Rex1–Rac1 signaling axis may be an adjunct therapy for treating invasive cancers which exhibit increased P-Rex1 expression.

Author contributions: N.S., H.-J.L., M.N., T.T., P.T., C.A.M., L.M.O., and C.A.M. designed research; N.S., H.-J.L., M.N., J.M., and L.M.O. performed research; H.Y.K.Y., A.P., H.E.A., K.I.A., and H.C.E.W. contributed new reagents/analytic tools; N.S., H.-J.L., M.N., J.M., L.M.O., and C.A.M. analyzed data; and N.S., L.M.O., and C.A.M. wrote the paper.

The authors declare no competing interest.

This article is a PNAS Direct Submission.

[1]N.S. and H.-J.L. contributed equally to this work.

[2]Present address: Pulmonary and Critical Care Medicine, Department of Medicine, Brigham and Women's Hospital, Harvard Medical School, Boston, MA 02115.

[3]L.M.O. and C.A.M. contributed equally to this work.

[4]To whom correspondence may be addressed. Email: christina.mitchell@monash.edu.

This article contains supporting information online at https://www.pnas.org/lookup/suppl/doi:10.1073/pnas.2006445117/-/DCSupplemental.

First published October 23, 2020.

study of the METABRIC dataset (n = 1,981) found a negative association between *PREX1* mRNA expression and outcome, and in this context, tumors expressing low levels of *PREX1* were more likely to have a shorter survival time compared to those with higher *PREX1* expression (16). A more recent study (n = 121 breast cancer samples) also showed that high levels of P-Rex1 protein expression was associated with longer disease-free survival in breast cancer (17). The reasons behind these conflicting reports are unclear, but it is possible that P-Rex1 mRNA and protein expression are not functionally equivalent in breast cancer or this may reflect differences in patient cohorts, cohort sizes, breast cancer subtypes, P-Rex1 antibody specificity, or other inherent differences between studies.

Experimental studies using immortalized breast cancer cell lines have demonstrated P-Rex1 promotes cell proliferation and migration and enhances xenograft tumor formation via activation of PI3K/AKT, Rac, and/or MEK/ERK signaling (10, 11, 13, 18). In addition, characterization of a breast cancer cell line established from bone-disseminated MCF-7 cells (MCF7b) identified P-Rex1 as an important mediator of breast cancer metastasis to bone (19). However, the only murine model of P-Rex1 overexpression, a transgenic mouse in which P-Rex1 was expressed in mammary epithelial cells, did not develop de novo tumorigenesis or any abnormalities (20). These studies suggest the role P-Rex1 plays in breast cancer may be more complex than its reported role in melanoma. P-Rex1 is not detected in adult human skin, but is significantly expressed in 80% of primary and metastatic melanoma, with the highest level of expression in lymph node metastases (21). *Prex1*$^{-/-}$ mice exhibit no difference in the incidence or growth of primary tumors when crossed with the metastatic melanoma model *Tyr::Nras*^{Q61K}*;Ink4a*$^{-/-}$, but demonstrate reduced metastasis to the lung, liver, and brain, associated with improved survival (21). To date, analogous experiments assessing the effect of *Prex1* ablation on murine oncogene-driven breast cancer models have not been reported.

As there are several conflicting reports of the role P-Rex1 plays in breast cancer biology and the impact of its expression on long-term outcome, here we undertook analysis of human breast cancer databases and gene arrays for *PREX1* mRNA expression in specific subtypes, correlating with survival outcome. Based on the results of this analysis, we then modeled these findings by generating multiple unique murine models with altered P-Rex1 expression in mammary ductal epithelial cells. These experiments were designed to answer the question of whether P-Rex1 either alone, or via cooperation with other oncogenes, contributes to mammary tumor initiation, growth, and/or progression to metastasis. Collectively, our study identifies a causal relationship between P-Rex1 expression and breast cancer initiation that is preceded by alterations to ductal apicobasal polarity and cellular hyperplasia. P-Rex1 cooperates with neu/HER2 to increase breast tumor initiation and the number of metastases, but not primary tumor growth. We conclude P-Rex1 can function as an oncogene in breast cancer, both alone and in cooperation with other oncogenes, and its expression in breast cancer can impact on long-term survival by enhancing metastasis.

Results

As there are conflicting reports in the literature of the relative expression of *PREX1* mRNA in breast cancer subsets, here we examined a publically available dataset and a commercial tissue array to evaluate *PREX1* mRNA expression and its potential impact on long-term outcome. To this end we examined *PREX1* mRNA expression in TissueScan Human Breast Cancer cDNA arrays I–IV (OriGene), which contain 16 "normal" breast tissues and 176 primary breast cancer samples. In addition, 1,904 cases from the METABRIC cohort (cBioPortal for Cancer Genomics) (22) were analyzed. We avoided the use of P-Rex1 antibodies, as we have demonstrated many cross-react with the highly related P-Rex2 which is also expressed in breast cancer (23, 24), which may account for the conflicting reports of P-Rex1 expression in various breast cancers. *PREX1* mRNA expression was significantly higher in ER^{+ve} and progesterone receptor (PR)-positive cancers relative to ER^{-ve} and PR^{-ve} tumors in both cohorts (*SI Appendix*, Fig. S1 *A* and *B*). Stratifying samples for breast cancer subtype revealed *PREX1* mRNA expression was significantly higher in luminal (ER^{+ve} and/or PR^{+ve}) versus triple negative (ER^{-ve}/PR^{-ve}/HER^{-ve})

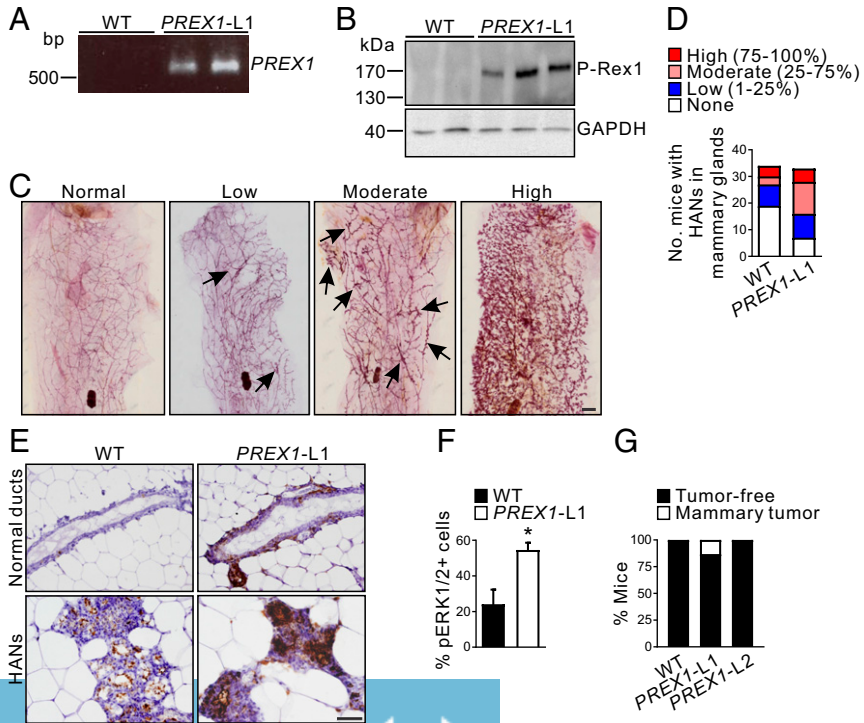

Fig. 1. High P-Rex1 expression enhances hyperplastic alveolar nodule formation and induces de novo mammary tumor formation in aged mice. (*A*) Identification of WT and MMTV-*PREX1* line 1 (*PREX1*-L1) transgenic mice by PCR of genomic DNA. (*B*) Whole-cell lysates from WT and MMTV-*PREX1*^{L1} transgenic mouse mammary epithelial cell organoids were immunoblotted with P-Rex1 or GAPDH antibodies. (*C*) Carmine alum-stained mammary gland whole mounts from 18- to 22-mo-old MMTV-*PREX1*^{L1} mice. Representative images of mammary glands with normal (0%), low (1 to 25%), moderate (25 to 75%), or high (75 to 100%) levels of HANs (arrows) are shown. (*D*) Data represent the number of 18- to 22-mo-old WT and MMTV-*PREX1*^{L1} mice with none, low, moderate, or high numbers of HANs in the mammary gland (WT n = 34, MMTV-*PREX1*^{L1} n = 33 mice). (*E*) Formalin-fixed, paraffin-embedded (FFPE) sections of mammary glands from 18- to 22-mo-old WT and MMTV-*PREX1*^{L1} mice were immunostained with pERK1/2 antibodies. (*F*) Quantitation of pERK1/2-positive epithelial cells in mammary ducts of 18- to 22-mo-old WT and MMTV-*PREX1*^{L1} mice. Data represent mean ± SEM (n = 5 mice/genotype, Student's t test). (*G*) Tumor incidence in 18- to 22-mo-old WT and MMTV-*PREX1* transgenic mice. Data represent the percentage of mice with or without mammary tumors (WT n = 50, MMTV-*PREX1*^{L1} n = 38, MMTV-*PREX1*^{L2} n = 19 mice). (Scale bars: 2 mm in *C*, 50 μm in *E*.) *P < 0.05.

cancers in the TissueScan arrays (*SI Appendix*, Fig. S1*A*). In the METABRIC cohort, *PREX1* mRNA expression was elevated in luminal A and B cancers relative to HER2^{+ve} or basal-like (ER^{-ve}/PR^{-ve}/HER^{-ve}) cancers (*SI Appendix*, Fig. S1*B*) although there was no difference in *PREX1* levels between luminal A versus luminal B cancers (*SI Appendix*, Fig. S1*B*). In addition, HER2^{+ve} tumors exhibited significantly higher *PREX1* mRNA levels relative to triple negative cancers (*SI Appendix*, Fig. S1*B*). To assess the effect of *PREX1* expression on disease-free (DFS) and distant disease-free survival (DDFS) in luminal breast cancers, the MTCI Breast Cancer Survival Analysis Tool (http://glados.ucd.ie/BreastMark/) was examined. High *PREX1* mRNA expression correlated with poor prognosis, including disease-free and distant disease-free survival in luminal B, which has a higher proliferative index, but not in luminal A breast cancers (*SI Appendix*, Fig. S1 *C* and *D*). Therefore, our analysis reveals a positive association between increased *PREX1* expression and ER^{+ve}/luminal breast cancers. Significantly, high *PREX1* mRNA in tumors correlates with poor long-term outcome in luminal B, but not luminal A breast cancers.

P-Rex1 Expression at High Levels Promotes De Novo Mammary Tumor Development, Preceded by Apical Ductal Polarity Defects. To experimentally determine if P-Rex1 directly plays a role in promoting breast cancer progression, we developed multiple unique murine models with increased, or loss of, P-Rex1 expression, in the presence or absence of expression of the HER2 homolog neu, given P-Rex1 is an essential mediator of ErbB signaling (10, 11). Mice with transgenic expression of P-Rex1 in mammary ductal epithelial cells were generated using a linearized MMTV-Myc-*PREX1* fragment (*SI Appendix*, Fig. S2*A*) and two independent MMTV-*PREX1* transgenic founder lines 1 and 2 (MMTV-*PREX1*^{L1} and ^{L2}) (Fig. 1*A* and *SI Appendix*, Fig. S2*B*) on a pure FVB/N background were characterized. Absolute levels of human *PREX1* transgene-derived mRNA and endogenous murine *Prex1* mRNA were each quantitated by droplet digital PCR using species-specific primers. Human *PREX1* transgene-derived mRNA was detected in MMTV-*PREX1* but not wild-type (WT) mammary epithelial cells (*SI Appendix*, Fig. S2*C*). Droplet digital PCR analysis revealed 66-fold higher Myc-*PREX1* transgene mRNA levels in line 1 versus line 2 mammary epithelial cells (*SI Appendix*, Fig. S2*C*). Human *PREX1* transgene expression in MMTV-*PREX1*^{L1} cells was not significantly different from endogenous *PREX1* mRNA levels in BT-474 or T47D ER^{+ve} human breast cancer cell lines (*SI Appendix*, Fig. S2*C*). Human *PREX1* transgene expression in MMTV-*PREX1*^{L2} cells was significantly higher than endogenous murine *Prex1* levels in wild-type mammary epithelial cells and endogenous *PREX1* levels in MCF-10A cells and ER^{-ve} breast cancer cell lines, but was lower than endogenous *PREX1* levels in T47D, BT-474, or MCF-7 ER^{+ve} breast cancer cell lines (*SI Appendix*, Fig. S2*C*). P-Rex1 antibody (18) immunoblot analysis revealed P-Rex1 expression in mammary organoid epithelial cells derived from MMTV-*PREX1*^{L1}, but not wild-type mice (Fig. 1*B*), which was restricted to ductal epithelial cells (*SI Appendix*, Fig. S2*D*). MMTV-*PREX1*^{L1} and ^{L2} mice were also crossed with the MMTV-*neu* mouse breast cancer model (25). Endogenous *Prex1* mRNA was expressed in both wild-type and MMTV-*neu* mouse mammary epithelial cells at comparable levels (*SI Appendix*, Fig. S2*E*). Droplet digital PCR analysis revealed endogenous *Prex1* mRNA levels were not altered by neu expression in MMTV-*neu* mammary tumor cells relative to wild-type mammary epithelial cells (*SI Appendix*, Fig. S2*F*). P-Rex1 protein was increased in mammary tumor cells from MMTV-*neu*;*PREX1*^{L1} and ^{L2} mice relative to MMTV-*neu* alone (*SI Appendix*, Fig. S2 *G* and *H*). The apparent discrepancy between P-Rex1 mRNA and protein expression in wild-type mammary epithelial cells may be due to protein levels being below the detection limit of the antibody. Previous studies have also reported no P-Rex1 protein expression in normal human mammary tissue (10, 11). Higher P-Rex1 protein was also observed in MMTV-*neu*;*PREX1*^{L1} compared to ^{L2} tumor derived cells (*SI Appendix*, Fig. S2 *G* and *H*) consistent with our mRNA analysis of mammary epithelial cells. P-Rex1 protein expression in MMTV-*neu*;*PREX1*^{L1} tumor cells was significantly lower than endogenous P-Rex1 protein levels in the ER^{+ve} T47D cell line (*SI Appendix*, Fig. S2 *G* and *I*). Collectively, these results suggest P-Rex1 was not overexpressed in mammary ductal epithelial cells more highly than in previously characterized immortalized breast cancer cell lines.

To determine whether P-Rex1 by itself can initiate de novo mammary tumorigenesis, nulliparous (virgin) wild-type and MMTV-*PREX1*^{L1} and ^{L2} transgenic mice were aged up to 22 mo. There is one previous reported study using a similar approach that expressed P-Rex1 in ductal epithelial cells, but these mice showed no tumor development after 1 y. Here we aged mice for longer, examined for a predisposition to hyperplasia, and also used two different transgenic lines with high versus low expression. Hyperplastic alveolar nodules (HANs) represent preneoplastic lesions with increased tumorigenic potential (26), but have also been observed at low levels in wild-type FVB/N mice as they age (27). MMTV-*PREX1*^{L1} mammary glands exhibited increased HANs compared to wild-type controls (Fig. 1 *C* and *D*, $P = 0.0055$, χ^2 test) with increased phosphorylation of ERK1/2 within MMTV-*PREX1*^{L1} HANs, relative to the HANs in wild-type mammary glands (Fig. 1*E*). P-Rex1 ectopic expression in MCF-7 and T47D human breast cancer cell lines promotes ERK1/2 (18, 28) but not AKT pathway signaling (10, 11, 18, 28). However, P-Rex1-dependent activation of ERK1/2 in breast cancer cells is contentious, as others reported that it does not enhance ERK pathway activation in MCF-7 cells (20). Here, morphologically normal MMTV-*PREX1* mammary ducts from aged mice displayed increased ERK1/2 phosphorylation compared to wild-type ducts (Fig. 1 *E* and *F*).

MMTV-*PREX1*^{L1}, ^{L2}, and wild-type mice were further monitored for de novo mammary tumor development for prolonged periods up to 22 mo of age. A total of 13% (5/38 mice) of MMTV-*PREX1*^{L1} mice developed palpable mammary tumors by 22 mo (Fig. 1*G*). No wild-type ($n = 50$) or MMTV-*PREX1*^{L2} mice ($n = 19$) developed palpable mammary tumors (Fig. 1*G*), suggesting a causal relationship between high levels of P-Rex1 expression and tumor initiation. Histological analysis of MMTV-*PREX1*^{L1} mammary tumors revealed a heterogeneous morphology with low grade areas comprising residual glandular structures (*SI Appendix*, Fig. S2*J*, *Bottom Right*) as well as areas of high grade tumor (*SI Appendix*, Fig. S2*J*). Many MMTV-*PREX1*^{L1} mammary tumor cells expressed the luminal marker cytokeratin 8 with some basal marker cytokeratin 14 staining (*SI Appendix*, Fig. S2*J*), suggesting a pluripotent progenitor cell origin (29). MMTV-*PREX1*^{L1} mammary tumors showed many proliferating Ki67-positive stained cells with prominent phosphorylated ERK1/2 and less intense pAKT staining (*SI Appendix*, Fig. S2*J*).

P-Rex1 Expression Disrupts Mammary Epithelial Cell Polarity during Development. The establishment of correct epithelial polarity is critical for mammary gland architecture and function, and the loss of epithelial cell polarity and growth control are characteristics of malignant tumors (30–32). Many of the molecular components required for normal mammary development are dysregulated in breast cancer (33, 34), therefore we determined whether P-Rex1 expression can affect these events. Mice are born with a rudimentary ductal tree that occupies a small portion of the mammary fat pad. During puberty, the ductal tree branches and extends throughout the mammary fat pad via proliferative terminal end buds (TEBs) until the whole fat pad is filled with a system of branched ducts (35). The Rac signaling pathway is required for murine mammary gland branching morphogenesis, regulating both branch initiation and extension (36). During mammary gland development, ductal epithelial cells also play a critical role

in side-branch formation (37). P-Rex1 regulation of ductal morphogenesis was examined in pubescent (4 and 7 wk) and adult (16 wk) MMTV-*PREX1*^{L1} transgenic virgin mice, but no difference in the invasion of the ductal tree into the mammary fat pad was detected (Fig. 2 *A* and *B*) with similar numbers of TEBs at 4 and 7 wk of age (Fig. 2 *A* and *C*). At 16 wk, the ductal tree in MMTV-*PREX1*^{L1} and wild-type mice had extended to fill the mammary fat pad (Fig. 2*A*) and no difference in ductal width was observed between the two genotypes (Fig. 2*D*). However, adult MMTV-*PREX1*^{L1} mammary glands exhibited significantly enhanced aberrant side branching with a 2.4-fold increase in the number of branch points per field relative to controls (Fig. 2 *A* and *E*).

To further characterize branching defects, organoid cultures were established by isolating ductal epithelial cells from MMTV-*PREX1*^{L1} and ^{L2} transgenic mice, which showed a more branched morphology when cultured in Matrigel compared to wild type (*SI Appendix*, Fig. S2 *K* and *L*). A small percentage (9%) of *PREX1*^{L1} organoids formed elongated branches which extended into the matrix (*SI Appendix*, Fig. S2 *K* and *L*). A mixed gel of 30% Matrigel:70% preassembled collagen 1 (3M7C) supports more organotypic branching with epithelial elongation analogous to TEBs in mammary glands (38). Under these conditions MMTV-*PREX1*^{L1} mammary organoids exhibited more extensively branched morphology than wild type (Fig. 2 *F* and *G*), with an increased number of pERK1/2-positive cells (Fig. 2 *H* and *I*). Interestingly the most prominent pERK1/2 staining was observed at the leading edge of the organoid branches.

Mouse mammary ducts are composed of a bilayered epithelium comprising luminal epithelial cells that show apicobasal polarization, surrounded by a basal myoepithelial layer. Luminal epithelial cells are cuboidal with centralized nuclei and little cytoplasm (39). MMTV-*PREX1*^{L1} mammary glands showed normal ductal morphology (Fig. 3*A*), with a layer of luminal lineage marker cytokeratin 8 (K8)-positive cells surrounded by basal/myoepithelial marker cytokeratin 14 (K14)-positive cells, similar to wild type (Fig. 3*B*). Mammary epithelial cell differentiation is characterized by the establishment of apicobasal polarity with specification of distinct apical and basolateral membranes (40, 41). Rac activity is required for E-cadherin junction formation, and constitutive activation of Rac induces disruption of E-cadherin junctions by promoting aberrant actin remodeling (42–44). Mammary ducts from two separate cohorts of wild-type mice displayed E-cadherin (adherens junction protein) staining on both basal and lateral membranes, and pERM (apical membrane marker) staining was restricted to apical membranes lining the lumen in 80 to 85% of ducts (Fig. 3 *C* and *D* and *SI Appendix*, Fig. S3). However, 50% of all MMTV-*PREX1*^{L1} and MMTV-*PREX1*^{L2} mammary ducts exhibited colocalization of the apical pERM marker with E-cadherin on the lateral and basal membranes (Fig. 3 *C* and *D* and *SI Appendix*, Fig. S3), consistent with an interpretation that P-Rex1 disrupts ductal apicobasal polarity. Notably, P-Rex1 increased cell proliferation in ducts at 16 wk as shown by Ki67 staining (line 1: 3.1-fold; line 2: 3.3-fold) (Fig. 3 *E* and *F* and *SI Appendix*, Fig. S4 *A* and *B*). However, no difference in apoptosis was detected by terminal deoxynucleotide transferase dUTP nick end labeling staining (*SI Appendix*, Fig. S4 *C* and *D*), revealing that P-Rex1 disrupts apicobasal polarity and promotes mammary epithelial cell proliferation, but does not influence apoptosis. Activated ERK1/2 regulates G1–S phase progression (45, 46). Here, a significant increase in ERK1/2 phosphorylation (2.6-fold) was observed in MMTV-*PREX1*^{L1} mammary ducts at both 7 and 16 wk of age (Fig. 3 *G* and *H*) and in MMTV-*PREX1*^{L2} ducts at 16 wk (*SI Appendix*, Fig. S4 *E* and *F*) compared to wild type.

To substantiate the observation that P-Rex1 disrupts apicobasal polarity, ectopic HA-tagged P-Rex1 was expressed using

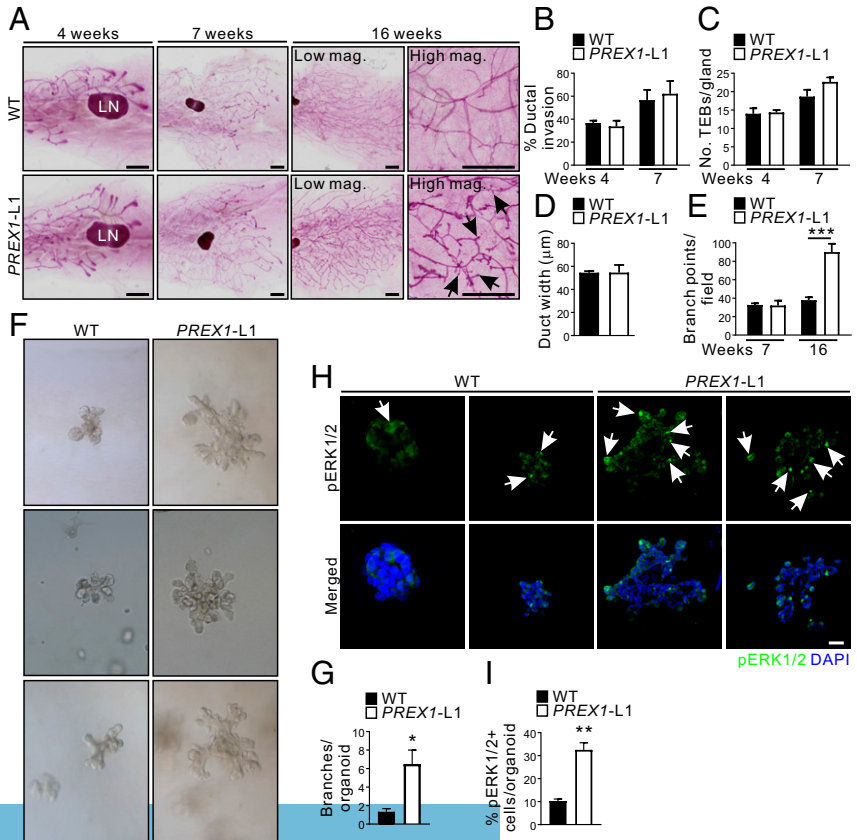

Fig. 2. P-Rex1 overexpression in the mammary gland alters branching morphogenesis. (*A*) Carmine alum-stained mammary gland whole mounts from 4-, 7-, and 16-wk-old virgin WT and MMTV-*PREX1*^{L1} mice. Arrows indicate aberrant side branches. (*B*) Data represent mean ductal invasion ± SEM in 4- and 7-wk-old WT and MMTV-*PREX1*^{L1} mice (n = 3 mice/genotype/time point; one-way ANOVA and Tukey's multiple comparisons test). (*C*). Data represent mean number of TEBs/gland ± SEM in 4- and 7-wk-old WT and MMTV-*PREX1*^{L1} mice (4 wk: WT n = 4 mice, MMTV-*PREX1*^{L1} n = 3 mice; 7 wk n = 3 mice/genotype; one-way ANOVA and Tukey's multiple comparisons test). (*D*) Data represent mean ductal width ± SEM in 16-wk-old WT and MMTV-*PREX1*^{L1} mice (n = 3 mice/genotype, 10 ducts/mouse, Student's t test). (*E*) Data represent the number of branch points/field ± SEM in 7- and 16-wk-old MMTV-*PREX1*^{L1} mice (n = 3 mice/genotype/time point; one-way ANOVA and Tukey's multiple comparisons test). (*F* and *G*) Mammary epithelial organoids from WT and MMTV-*PREX1*^{L1} mice were cultured in 30% Matrigel:70% collagen 1 (*F*). Data represent the number of branches/organoid ± SEM (n = 3 mice/genotype, >20 organoids/mouse, Student's t test) (*G*). (*H* and *I*) Formalin-fixed, paraffin-embedded sections of mammary epithelial organoids from WT and MMTV-*PREX1*^{L1} mice cultured in 30% Matrigel:70% collagen 1 were immunostained with a pERK1/2 antibody (arrows) and DAPI (*H*). Data represent mean percentage of pERK1/2-positive cells/organoid ± SEM (*I*) (n = 3 mice/genotype, >10 organoids/mouse, Student's t test). (Scale bars: 2 mm in *A*, 100 μm in *F*, and 50 μm in *H*.) *P < 0.05, **P < 0.01, ***P < 0.001.

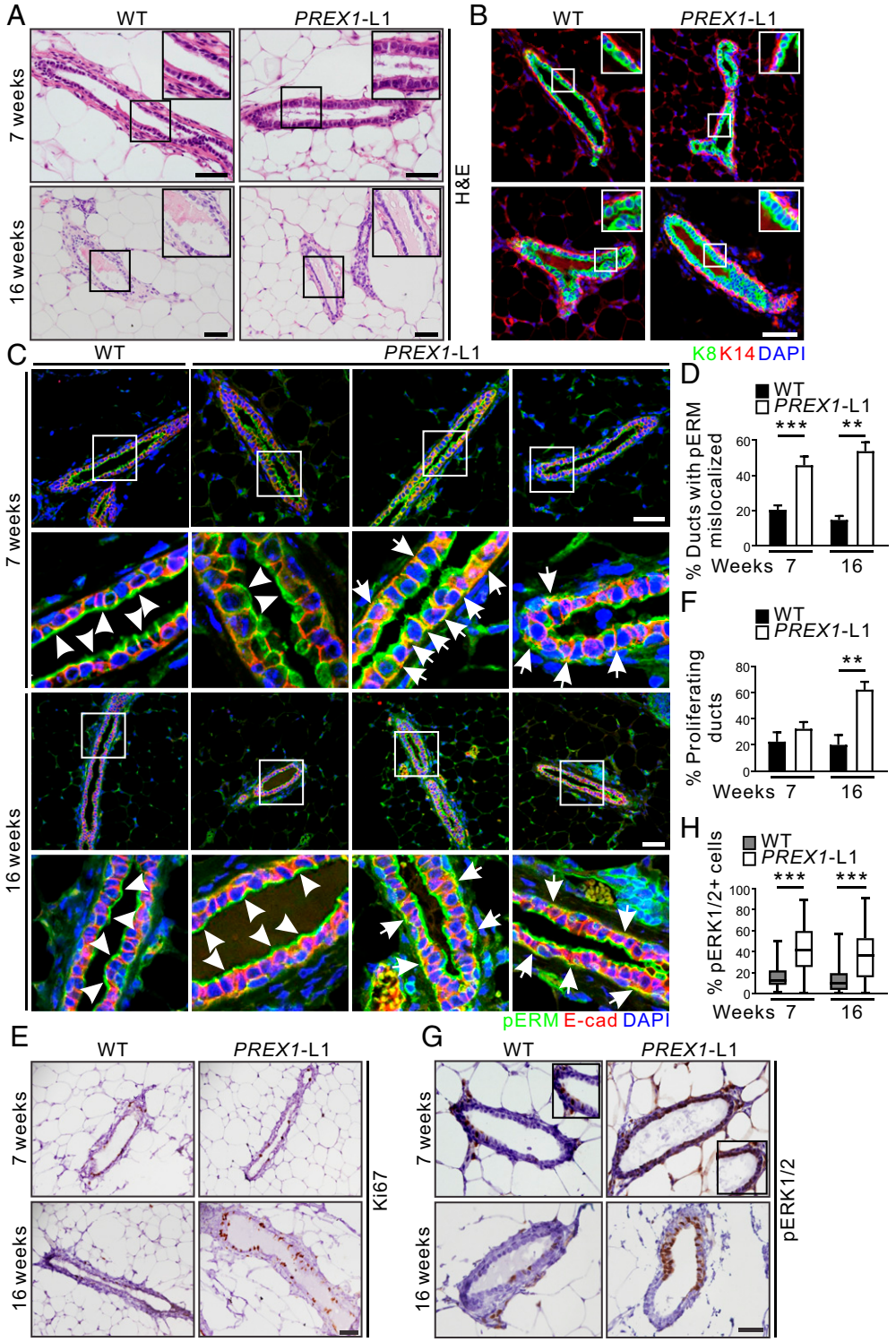

Fig. 3. P-Rex1 overexpression disrupts mammary epithelial cell polarity. (*A*) Formalin-fixed, paraffin-embedded (FFPE) sections of mammary glands from 7- and 16-wk-old WT and MMTV-*PREX1*^{L1} mice stained with H&E. (*B*) FFPE sections of mammary glands from 7- and 16-wk-old WT and MMTV-*PREX1*^{L1} mice immunostained with K8 (luminal marker) and K14 (basal marker) antibodies and DAPI. (*C* and *D*) FFPE sections of mammary glands from 7- and 16-wk-old WT and MMTV-*PREX1*^{L1} mice were immunostained with pERM and E-cadherin antibodies and DAPI. Higher power images of the boxed regions are shown (*Lower*). Representative images show normal (white arrowheads) and mislocalized (white arrows) pERM staining in mammary ducts (*C*). Data represent the mean percentage of ducts with mislocalized pERM ± SEM (7 wk: WT $n = 7$, MMTV-*PREX1*^{L1} $n = 7$; 16 wk: $n = 4$ mice/genotype, >100 ducts/mouse; one-way ANOVA and Tukey's multiple comparisons test) (*D*). (*E* and *F*) FFPE sections of mammary glands from 7- and 16-wk-old WT and MMTV-*PREX1*^{L1} mice were stained with a Ki67 antibody (*E*). Data represent mean ± SEM (7 wk: WT $n = 7$ mice, MMTV-*PREX1*^{L1} $n = 8$ mice; 16 wk: WT $n = 5$ mice, MMTV-*PREX1*^{L1} $n = 4$ mice, >15 ducts/mouse; one-way ANOVA and Tukey's multiple comparisons test) (*F*). (*G* and *H*) FFPE sections of mammary glands from 7- and 16-wk-old WT and MMTV-*PREX1*^{L1} mice were immunostained with a pERK1/2 antibody (*G*). Data represent mean percentage of pERK1/2-positive epithelial cells ± SEM (7 wk: $n = 3$ mice/genotype, 16 wk: $n = 5$ mice/genotype; >1,500 mammary epithelial cells from four random sections were analyzed per mouse; one-way ANOVA and Tukey's multiple comparisons test) (*H*). (Scale bars: 50 μm.) $^{**}P < 0.01$, $^{***}P < 0.001$.

a Tet-On 3G doxycycline-inducible expression system in the nontransformed mammary epithelial cell line MCF-10A. Expression levels were similar to endogenous P-Rex1 in ER^{+ve} MCF-7 breast cancer cells (*SI Appendix*, Fig. S5*A*). Control vector cells formed mature acini with a single layer of epithelial cells surrounding a hollow lumen (*SI Appendix*, Fig. S5*B*). In contrast, HA-PREX1-expressing acini were disorganized and a lumen was not formed even after 21 d in culture. In addition, 35 to 50% of acini exhibited actin-rich protrusions extending away from the main body of the acinus (*SI Appendix*, Fig. S5*B*), reminiscent of the extensions formed in MCF-10A and MDCK cysts undergoing HGF- or Raf-MEK-ERK-induced branching tubulogenesis (47–49). HA-PREX1 acini showed increased Ki67-positive cells compared to vector controls (1.76-fold in day-7 and 3.9-fold in day-14 acini) (*SI Appendix*, Fig. S5*C*). By day 21, MCF-10A vector-control acini cells had ceased proliferating, but HA-PREX1 acini cells continued to proliferate, albeit to a lesser extent than earlier time points (*SI Appendix*, Fig. S5*C*). No significant differences in apoptotic cells were observed (*SI Appendix*, Fig. S5*D*), suggesting that P-Rex1 does not regulate apoptosis in this context, similar to our observations in vivo. MCF-10A acini are polarized structures, with nuclei located at the basolateral pole and Golgi located apically above the nucleus (50). The outer layer of cells in HA-PREX1 acini exhibited nuclei localized to the middle or apical, rather than at the basal pole as observed in control cells (*SI Appendix*, Fig. S5 *B* and *E*). In addition the Golgi body localized at the side of the nucleus facing the lumen in most vector control acinar cells (*SI Appendix*, Fig. S5 *F* and *G*), but showed abnormal orientation upon ectopic P-Rex1 expression (19.1% cells versus 2% of vector controls) (*SI Appendix*, Fig. S5 *F* and *G*), suggesting a polarity defect. Collectively these results suggest P-Rex1 expression in mammary ductal epithelium disrupts ductal cell polarity, leading to mammary hyperplasia and, its expression at high levels can induce de novo tumorigenesis.

***Prex1* Ablation Confers a Survival Advantage in Oncogene-Driven Murine Models of Breast Cancer.** We next examined the effects of P-Rex1 overexpression on mammary tumorigenesis in an oncogene-driven context. In breast cancer cell lines, signals from ErbB receptors and GPCRs converge on P-Rex1 to mediate Rac1 activation (10, 11). To examine these functional interactions in vivo, *Prex1*$^{-/-}$ mice were crossed with MMTV-*neu* mice; the latter strain expresses wild-type neu in mammary epithelial cells under the control of the MMTV promoter, a well-characterized model of HER2-driven mammary carcinogenesis (25). *Prex1*$^{-/-}$ mice exhibit skin depigmentation, mild neutrophilia, and defective neutrophil accumulation at sites of inflammation (21, 51). MMTV-*neu* mice develop mammary adenocarcinomas from ∼4 to 7 mo of age (25, 52). *Prex1*$^{-/-}$ mice were also crossed with MMTV-*PyMT* mice; the latter murine model exhibits features of the ER^{+ve} luminal subtype with activation of PI3K signaling (53, 54). These breast cancer mouse models were engineered to also express the Raichu-Rac FRET biosensor in all tissues to assess Rac activation (55). Homozygous loss of *Prex1* significantly extended the time to reach clinical endpoint, defined as the primary tumor reaching a diameter of 1.5 cm, in both Rac1-FRET;MMTV-*neu* and Rac1-FRET;MMTV-*PyMT* breast cancer models (Fig. 4 *A* and *B*). Heterozygous *Prex1* ablation conferred a significant survival advantage to Rac1-FRET;*PyMT*, but not Rac1-FRET;*neu* mice (Fig. 4 *A* and *B*). In control studies, immunohistochemical staining of Rac1-FRET;MMTV-*neu* and Rac1-FRET;MMTV-*PyMT* mammary tumor sections revealed similar expression of the neu and PyMT transgenes, respectively, in *Prex1*$^{+/+}$, *Prex1*$^{+/-}$, and *Prex1*$^{-/-}$ tumors (*SI Appendix*, Fig. S6 *A* and *B*).

P-Rex1 acts as a Rac-GEF that increases Rac1 GTPase activation, including in breast cancer MDA-MB-231 cells but whether this occurs in the mammary gland has not been demonstrated as

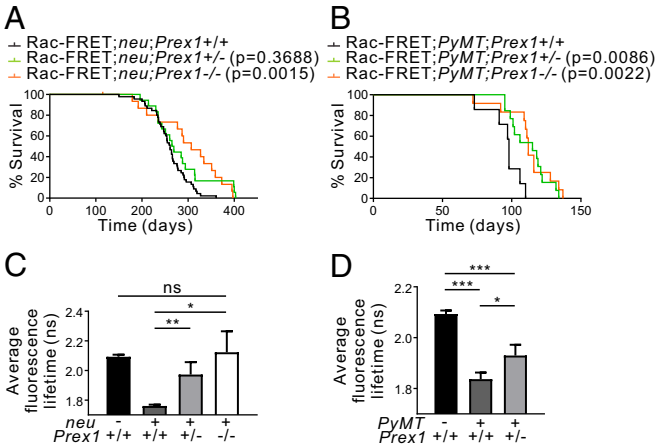

Fig. 4. *Prex1* ablation increases survival in oncogene-driven mouse models of breast cancer. (*A* and *B*) Kaplan–Meier survival curves of (*A*) Rac1-FRET;*neu* (n = 45), Rac1-FRET;*neu;Prex1*$^{+/-}$ (n = 18), Rac1-FRET;*neu;Prex1*$^{-/-}$ (n = 16) mice, and (*B*) Rac1-FRET;*PyMT* (n = 7), Rac1-FRET;*PyMT;Prex1*$^{+/-}$ (n = 13), Rac1-FRET;*PyMT;Prex1*$^{-/-}$ (n = 12) mice showing *Prex1* loss significantly increases survival to endpoint (primary tumor ≥1.5 cm diameter) (Log-rank Mantel–Cox test). (*C–D*) Rac1-FRET;*neu;Prex1* (*C*) or Rac1-FRET;*PyMT;Prex1* (*D*) mice at clinical endpoint were imaged on a multiphoton system. Quantitation of average fluorescence lifetimes of individual cells inside the primary tumor mass at clinical endpoint. Data represent mean fluorescence lifetime ± SD [n = 3 mice/genotype, (*C*) 257 cells, (*D*) 264 cells] (one-way ANOVA and Tukey's multiple comparisons test). *P < 0.05, **P < 0.01, ***P < 0.001, ns, not significant.

P-Rex1 expression is negligible in the normal breast (10, 11). To explore whether P-Rex1 can activate Rac1 in vivo in the mammary gland, Rac1-FRET;*Prex1*$^{+/+}$, Rac1-FRET;*neu;Prex1*, and Rac1-FRET;*PyMT;Prex1* mice were imaged live using multiphoton microscopy of exposed mammary gland (Rac1-FRET;*Prex1*$^{+/+}$ mice) or tumor tissue at clinical endpoint (Rac-FRET;*neu;Prex1* and Rac-FRET;*PyMT;Prex1* mice with a primary mammary tumor of 1.5-cm diameter). Rac1 activity was measured by fluorescence lifetime imaging microscopy-Förster resonance energy transfer (FLIM-FRET) of the donor fluorophore CFP which decreases upon FRET. In this model, active Rac1 results in lower fluorescence lifetime of the donor and for inactive Rac1 the fluorescence lifetime of the CFP is higher (*SI Appendix*, Fig. 6*C*). High CFP fluorescence lifetime (red/yellow in the FLIM heatmaps) which corresponds to low Rac1 activity was detected in the mammary glands of Rac1-FRET;*Prex1*$^{+/+}$ mice consistent with reports of low P-Rex1 expression in normal mammary tissue. Enhanced Rac1 activity is observed downstream of various oncogenes such as HER2 (ErbB2/neu), as a result of increased activation of PI3K, which then activates Rac-GEFs such as P-Rex1 (6, 10, 13). Consistent with this, high Rac1 activity (blue in the FLIM heatmaps) was readily detected in primary mammary tumor tissue of Rac1-FRET;MMTV-*neu* and Rac1-FRET;MMTV-*PyMT* mice (Fig. 4 *C* and *D* and *SI Appendix*, Fig. S6 *D* and *E*). Reduced Rac1 activity was observed in Rac1-FRET;MMTV-*neu* and Rac1-FRET;MMTV-*PyMT* tumors with heterozygous loss of *Prex1*, compared to Rac1-FRET;MMTV-*neu;Prex1*$^{+/+}$ and Rac1-FRET;MMTV-*PyMT;Prex1*$^{+/+}$ tumors (Fig. 4 *C* and *D* and *SI Appendix*, Fig. S6 *D* and *E*). Rac1-FRET;MMTV-*neu* tumors with homozygous *Prex1* ablation exhibited Rac1 activation similar to the basal levels observed in wild-type mammary glands (Fig. 4 *C* and *SI Appendix*, Fig. S6*D*). We conclude P-Rex1 activates Rac1 downstream of HER2 or PI3K in vivo in mammary tumors, and loss of P-Rex1 expression reduces Rac1 activation, correlating with enhanced long-term survival of oncogene-driven breast cancer model mice.

P-Rex1 Cooperates with HER2/Neu to Increase Mammary Tumor Incidence and the Number of Metastases. P-Rex1 mediates cell proliferation and migration downstream of HER receptors (10) and, as shown here, high *PREX1* mRNA expression correlates with impaired survival of luminal B breast cancer cohorts, which may be HER2^{+ve} (*SI Appendix*, Fig. S1 *C* and *D*). We next determined if P-Rex1 can enhance mammary tumor progression in cooperation with HER2/neu. To this end MMTV-*PREX1*^{L1} and ^{L2} mice were crossed with MMTV-*neu* breast cancer model mice. Immunohistochemical staining of tumor sections revealed similar expression of the neu oncogene in MMTV-*neu*, MMTV-*neu;PREX1*^{L1}, and ^{L2} mammary tumors (*SI Appendix*, Fig. S7*A*). Mice were monitored for tumor incidence by physical palpation and visual inspection, and tumor-free survival was assessed by Kaplan–Meier analysis. MMTV-*neu;PREX1* transgenic mice showed significantly increased mammary tumor incidence, defined as the percentage of mice developing a mammary tumor within the first year of life (MMTV-*neu* 58%, MMTV-*neu;PREX1*^{L1} 87% P = 0.0019, MMTV-*neu;PREX1*^{L2} 84% P = 0.0096) (Fig. 5*A* and *SI Appendix*, Fig. S7*B*), and showed reduced tumor-free survival (median tumor-free survival 281 d for MMTV-*neu;PREX1*^{L1} mice P = 0.0012, 278 d for MMTV-*neu;PREX1*^{L2} mice P = 0.0199) compared to MMTV-*neu* mice (median tumor-free survival 321 d) (Fig. 5*B* and *SI Appendix*, Fig. S7*C*). However, tumor growth, scored by the volume of the largest tumor per mouse, was not different between MMTV-*neu;PREX1* relative to MMTV-*neu* mice (Fig. 5*C* and *SI Appendix*, Fig. S7*D*). In addition, cell proliferation in established tumors (500-mm^3 or advanced 1,000-mm^3 tumors) was equivalent (Fig. 5*D*). These results suggest that P-Rex1 promotes mammary tumor initiation, but once tumors are established does not contribute to tumor growth in the presence of the neu oncogene. Endogenous *Prex1* mRNA expression was not altered in MMTV-*neu* tumor cells relative to wild-type mammary epithelial cells (*SI Appendix*, Fig. S2*F*); therefore, the lack of difference in proliferation and tumor growth is unlikely to be due to a spontaneous increase in endogenous *Prex1* expression in MMTV-*neu* tumors. Immunohistochemical analysis using cytokeratin 8 and 14 antibodies confirmed MMTV-*neu* and MMTV-*neu;PREX1*^{L1} mammary tumors were of luminal epithelial cell origin (Fig. 5*E*), and phosphorylation of ERK1/2, S6, 4EB-P1, or AKT or expression of cyclin D1 in 500-mm^3 mammary tumors appeared equivalent (Fig. 5 *F* and *G*). No difference in pERK1/2 or pS6 staining was observed in advanced tumors (*SI Appendix*, Fig. S7 *E* and *F*), suggesting these signaling pathways may be maximally activated by neu, and not further increased by concomitant expression of P-Rex1 in established tumors. Very few apoptotic cells were detected by cleaved caspase 3 staining in either MMTV-*neu* or MMTV-*neu;PREX1*^{L1} advanced tumors (*SI Appendix*, Fig. S7 *E*).

To further characterize P-Rex1's role in mammary tumorigenesis, cells were isolated from MMTV-*neu* and MMTV-*neu;PREX1* primary mammary tumors, plated as single cells in Matrigel and cultured for 10 or 14 d to form tumoroids. MMTV-*neu;PREX1*^{L1} and, to a lesser extent, ^{L2} tumor cells formed increased numbers of tumoroids that were also larger compared to MMTV-*neu*-derived tumor cells (Fig. 6 *A–C* and *SI Appendix*, Fig. S8 *A–C*), but individual tumoroids showed no difference in cell proliferation (Fig. 6 *D* and *E*). These results are consistent with an interpretation that P-Rex1 enhances the early initiation stage of tumoroid formation and therefore established MMTV-*neu;PREX1* tumoroids are larger than MMTV-*neu* colonies at

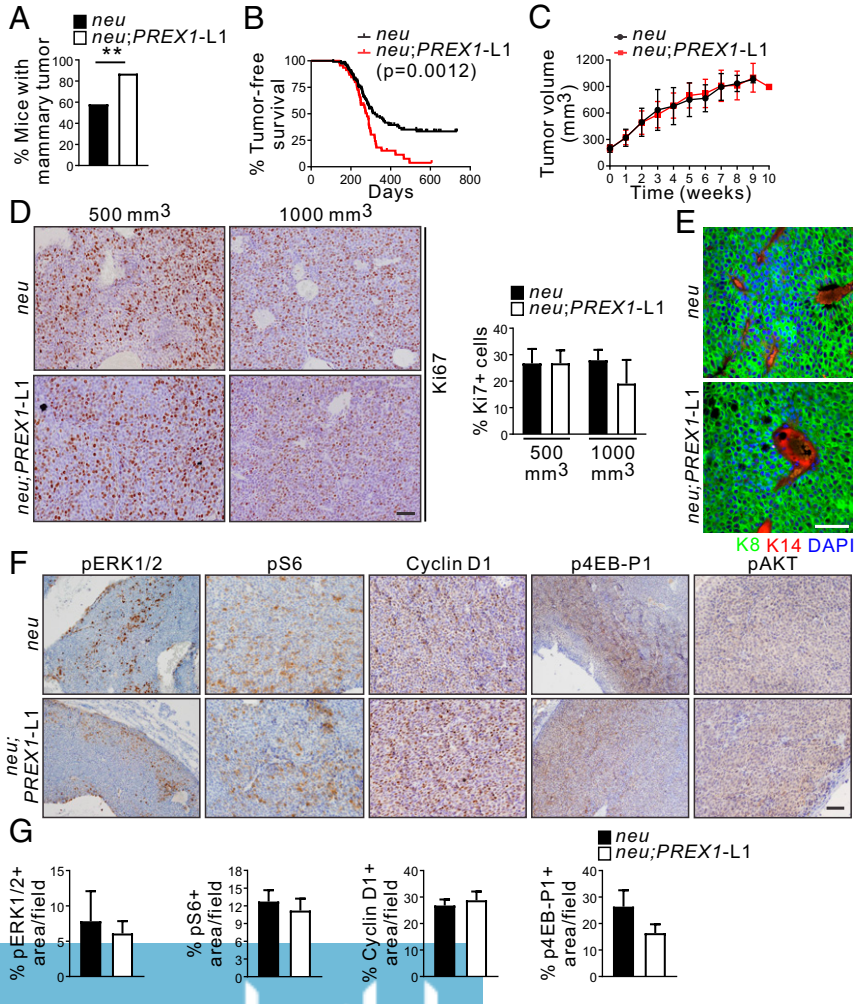

Fig. 5. P-Rex1 overexpression enhances tumor initiation in an oncogene-driven mouse model of breast cancer. (*A*) Data show tumor incidence defined as the percentage of MMTV-*neu* (n = 93) and MMTV-*neu;PREX1*^{L1} (n = 38) (χ^2 test) mice developing a palpable mammary tumor within the first year of life. (*B*) Kaplan–Meier curve showing tumor-free MMTV-*neu* (n = 117) and MMTV-*neu;PREX1*^{L1} (n = 46) mice (Log-rank Mantel–Cox test). (*C*) Data represent mean tumor volume (mm^3) ± SEM after diagnosis (time 0) from MMTV-*neu* (n = 38) and MMTV-*neu;PREX1*^{L1} mice (n = 23). The largest tumor in all mice exhibited similar sizes (100 to 200 mm^3) at diagnosis. (*D*) Formalin-fixed, paraffin-embedded (FFPE) sections of 500-mm^3 and 1,000-mm^3 mammary tumors from MMTV-*neu* and MMTV-*neu;PREX1*^{L1} mice were immunostained with Ki67 antibodies and scored for the presence of Ki67-positive cells. Data represent mean ± SEM (MMTV-*neu* n = 3, MMTV-*neu;PREX1*^{L1} n = 4 mice, >10,000 cells/mouse; one-way ANOVA and Tukey's multiple comparisons test). (*E*) Mammary tumoroids from MMTV-*neu* and MMTV-*neu;PREX1*^{L1} transgenic mice immunostained with K8 and K14 antibodies and DAPI. (*F* and *G*) FFPE sections of 500-mm^3 mammary tumors from MMTV-*neu* and MMTV-*neu;PREX1*^{L1} mice immunostained with pERK1/2, pS6, cyclin D1, p4EB-P1, or pAKT antibodies (*F*). Data represent the mean percentage of positive area/field ± SEM (>10,000 cells/mouse) (*G*). (Scale bars: 50 μm in *D–F*.) **P < 0.01.

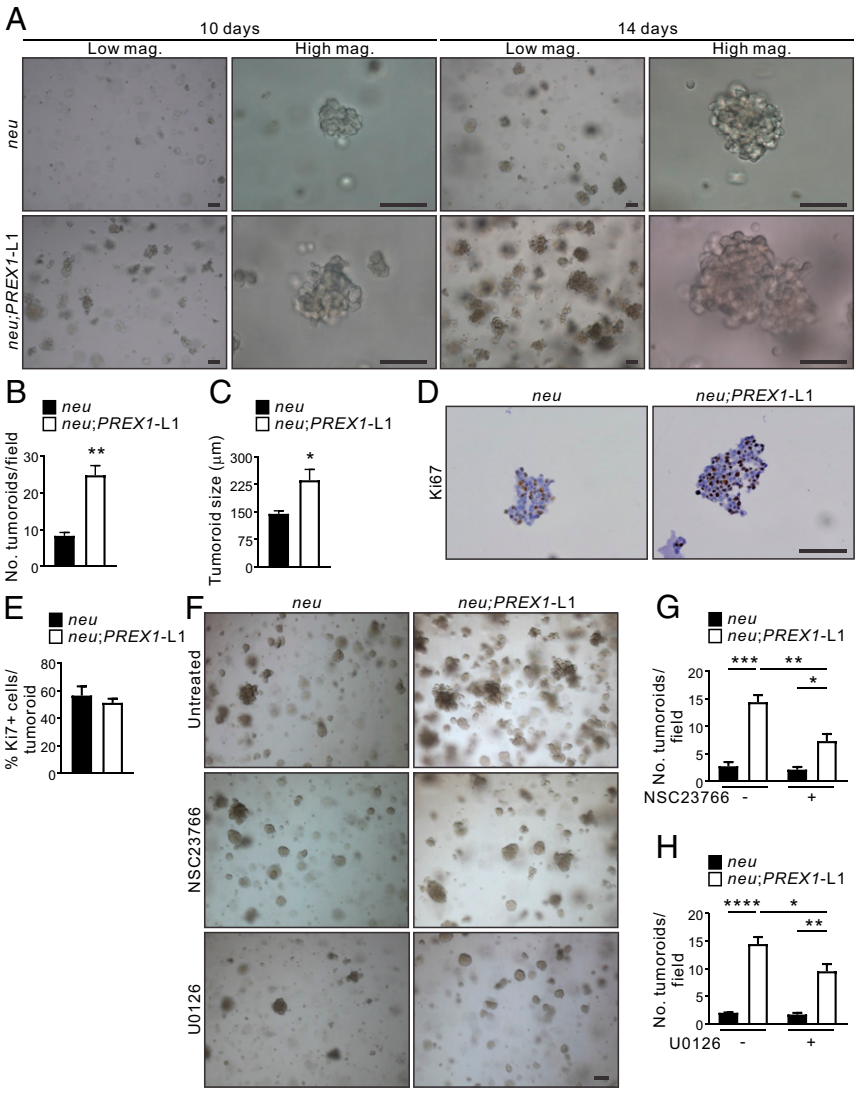

Fig. 6. P-Rex1 enhances mammary tumoroid colony formation in a Rac1-dependent manner. (*A–C*) Mammary tumoroids from MMTV-*neu* and MMTV-*neu;PREX1*^{L1} transgenic mice were cultured in Matrigel for 10 or 14 d and imaged by brightfield microscopy (*A*). Data represent mean number of tumoroids/field ± SEM (n = 3 mice/genotype, >5 fields/genotype) (*B*) or mean tumoroid size ± SEM (n = 3 mice/genotype, >12 tumoroids; Student's t test) (*C*). (*D* and *E*) Sections from 14-d formalin-fixed, paraffin-embedded mammary tumoroids from MMTV-*neu* and MMTV-*neu;PREX1*^{L1} mice were immunostained with a Ki67 antibody (*D*). Data represent mean Ki67^{+} cells/tumoroid ± SEM (n = 3 mice/genotype, >15 tumoroids/mouse; Student's t test) (*E*). (*F–H*) Mammary tumoroids from MMTV-*neu* and MMTV-*neu;PREX1*^{L1} mice were cultured in Matrigel ± 5 μM NSC23766 or 0.5 μM U0126 for 14 d (*F*). Data represent mean number of tumoroids/field ± SEM in untreated versus tumoroids treated with NSC23766 (*G*) or U1026 (*H*) (n = 3 mice/genotype, >5 fields/genotype; two-way ANOVA and Tukey's multiple comparisons test). (Scale bars: 100 μm.) *P < 0.05, **P < 0.01, ***P < 0.001, ****P < 0.0001.

the 10- and 14-d time points. Pharmacological inhibition of Rac1 (5 μM NSC23766) or MEK1/2 (0.5 μM U0126) rescued the enhanced colony formation of MMTV-neu;*PREX1*^{L1} and ^{L2} tumoroids (Fig. 6 *F–H* and *SI Appendix*, Fig. S8 *D–F*), but at these concentrations had little effect on MMTV-*neu* tumoroids. These results are consistent with an interpretation that P-Rex1 expression promotes the initiation, but not the growth of established tumors downstream of the neu oncogene.

P-Rex1 Expression Promotes Mammary Tumor Invasion in a Rac-Dependent Manner. Metastasis is the major cause of breast cancer-related death. Increased P-Rex1 protein expression has been identified in metastatic human breast tumors and associated lymph node metastases, metastatic melanoma, and prostate tumors compared to primary tumors (10, 21, 56). *Prex1* knockout in a mouse model of melanoma (*Tyr*::*Nras*$^{Q61K/°}$ transgenic mice) reduced melanoma metastasis (21), but whether P-Rex1 promotes metastatic dissemination in breast cancer is unknown. Here we assessed the contribution P-Rex-1 plays in murine breast cancer metastasis. Approximately 70% of MMTV-*neu* mice over 8 mo of age develop lung metastases (25) and coexpression of P-Rex1 expression did not affect this outcome. However, the total number of lung metastases was significantly higher in MMTV-*neu;PREX1*^{L1} versus MMTV-*neu* mice (5.8-fold increase, P < 0.05) (Fig. 7 *A–C*), suggesting that P-Rex1 expression increases the number of metastases, even when primary tumors are of equivalent size.

P-Rex1 regulation of breast cancer cell migration and invasion was also assessed in vitro using Transwell assays. Mammary epithelial cell lines established from MMTV-*neu;PREX1*^{L1} primary mammary tumors showed a 2.1-fold increase in migration toward a chemoattractant (fetal calf serum), relative to MMTV-*neu* tumor cells (Fig. 7 *D* and *E*) and also displayed an enhanced ability to invade through Matrigel toward a chemoattractant (*SI Appendix*, Fig. S9*A*). Mammary tumor cells derived from MMTV-*neu;PREX1* and MMTV-*neu* mice were embedded in a 3D type I collagen matrix and grown to form tumoroids. MMTV-*neu;PREX1* cells showed enhanced formation of larger colonies relative to MMTV-*neu* alone, and notably increased migration and invasion of tumor cells from colonies into the matrix were observed (Fig. 7 *F* and *G* and *SI Appendix*, Fig. S9*B*). MMTV-*neu;PREX1*^{L1} and ^{L2} mammary tumoroids exhibited higher levels of phosphorylated ERK1/2 relative to MMTV-*neu* tumoroids (Fig. 7 *H* and *I* and *SI Appendix*, Fig. S9 *C* and *D*). Significantly, migration of cells from MMTV-*neu;PREX1*^{L1} tumoroids was reduced by treatment with either Rac1 (5 μM NSC23766) or MEK1/2 (0.5 μM U0126) inhibitors (Fig. 7 *J* and *K*). Collectively, these data reveal P-Rex1 enhances neu-driven cancer cell migration and invasion, leading to an increased number of metastases, despite having no impact on established primary tumor growth.

Discussion

High P-Rex1 protein expression in breast cancer cohorts has been linked to decreased disease-free survival (11); however, paradoxically other reports propose the opposite finding for unknown reasons (16, 17). The in vivo function of P-Rex1 in the mammary gland has only been tested in one transgenic murine mouse model, which showed no causal association with tumor development. Here we report high *PREX1* mRNA expression is associated with reduced long-term survival only in luminal B breast cancers. Transgenic P-Rex1 expression in murine mammary ductal epithelial cells enhanced aberrant mammary ductal side branching, increased epithelial cell proliferation and hyperplasia, and at high levels induced de novo mammary tumors, providing evidence that P-Rex1 can play a direct causal role in breast tumor initiation. *Prex1* knockout in the MMTV-*neu* murine model of breast cancer reduced Rac1 activation and enhanced long-term survival. In contrast, coexpression of P-Rex1 with the neu oncogene in mammary epithelial cells increased tumor incidence and the number of metastases; however, the growth of established tumors was not affected. Significantly, Rac inhibition reduced the migration and invasion of mammary tumor cells derived from MMTV-*neu;PREX1* mice. Taken together our results reveal P-Rex1, either alone or in cooperation with other oncogenes such as HER2/neu, can increase tumor incidence and accelerate metastasis leading to reduced long-term outcomes, despite having no effect on established tumor growth. This may in part explain the conflicting long-term outcome results that have been reported, as P-Rex1 itself may have no direct effect on tumor growth, but in some breast cancer subtypes may increase the incidence of tumor initiation and spread of invasive tumors. It is interesting to speculate that the breast cancer subtype, the level of P-Rex1 expression, and/or the timing of this increased expression may impact on long-term outcome. The enhanced metastatic potential of the P-Rex1–Rac1 signaling pathway as reported here, suggests inhibition of this pathway may be an option for adjunct therapy for some P-Rex1-positive invasive breast cancers.

There are many possible confounding reasons for the significant differences in predictive outcome reported by various studies that have evaluated P-Rex1 expression in human breast cancer cohorts. Here increased *PREX1* mRNA expression was significantly associated with lower disease-free and distant disease-free survival in luminal B ($n = 545$ DFS, 191 DDFS), but not luminal A ($n = 429$ DFS, 241 DDFS) or other breast cancer subsets, consistent with the reduced tumor-free survival and enhanced metastasis observed in MMTV-*neu;PREX1* mice. Our findings are of interest as most previous studies did not examine patient survival in a breast cancer subtype-specific context (10–12, 16, 17), and those that examined protein expression analyzed only small cohort numbers. We acknowledge the limitation of our study in that we could not examine P-Rex1 protein expression, due to significant antibody cross-reactivity with the highly related P-Rex2. We speculate that previous studies should be interpreted with caution unless P-Rex1 versus P-Rex2 antibody cross-reactivity was tested and excluded. These two proteins exhibit a similar domain structure and 59% amino acid identity and P-Rex2 is reported to be expressed in all breast cancer subsets (7, 23).

To delineate the functional role P-Rex1 plays in breast cancer, we developed multiple unique mouse models of P-Rex1 loss, or ectopic expression in mammary ductal epithelial cells, in the presence or absence of other oncogenes, such as neu or PyMT. *Prex1* ablation conferred a survival advantage in neu and PyMT oncogene-driven murine models of breast cancer, reminiscent of its role in murine melanoma models (21). We also report that high P-Rex1 expression demonstrated a causal relationship with mammary cancer initiation. Recently, a mammary-specific P-Rex1 transgenic mouse on an FVB/N background was reported that showed no gross defects in mammary gland architecture or de novo tumor development (20). However, in this latter study, examination of ductal branching via whole mount analysis, apicobasal marker characterization of ductal epithelial cells, or cell proliferation studies were not reported, and mice were only monitored for tumor formation for 13 mo, unlike the 22 mo observation undertaken in our study. Furthermore, the consequences of transgenic P-Rex1 overexpression in the mammary gland were not assessed in the context of HER2/neu oncogene-driven tumors as examined here. It is also possible that variations in P-Rex1 transgene expression may account for the differences in phenotype between these two studies.

Our study revealed the interesting findings that P-Rex1 affects mammary ductal apicobasal polarity leading to defects in mammary branching morphogenesis, enhanced cell proliferation, and de novo cancer formation. Creation of a tubular architecture such as a mammary duct requires coordination of cell migration, proliferation, differentiation, and polarization (48). In early tubulogenesis, cells form invasive, actin-rich extensions that develop into single-file chains of cells that lose apicobasal polarity and acquire leading edge-trailing edge polarity typical of motile cells. Pharmacological inhibition of either Rac1 or MEK/ERK1/2 signaling blocks mammary epithelial cell migration and duct elongation (36). Interestingly, expression of constitutively active MEK1, but not Rac1, is sufficient to induce duct initiation and elongation (36). Although ERK activation is necessary and sufficient for the initial stage of tubulogenesis, it is dispensable in the latter stage when cells repolarize and differentiate (48, 57). In our study, 3D-morphogenesis assays revealed P-Rex1 promoted extensive actin rich protrusions from acini, organoid branching, and enhanced Rac1- and MEK1/2-dependent tumor cell migration. Both Rac1 and ERK1/2 are activated at the leading edge of branches (36, 58). We observed increased ERK1/2 signaling in P-Rex1 transgenic mammary ducts and enhanced ERK1/2 phosphorylation in P-Rex1 transgenic-derived mammary organoids, specifically at the leading edge of protrusions. However, we did not observe this in established MMTV-*neu;PREX1* mammary tumors, suggesting P-Rex1-driven ERK1/2 activation is context dependent and/or ERK1/2 is already maximally activated by the neu oncogene which is not synergistically further activated by P-Rex1.

Although no major structural changes were observed in MMTV-*neu;PREX1*^{L1} mammary ducts, such as cell multilayering, mislocalization of pERM was observed in mammary epithelial cells. Mammary epithelial cells exhibit reversible, incomplete apicobasal polarity and increased migration during branching morphogenesis which drives tube elongation (59). ERM proteins act downstream of Rho GTPases such as Rac to regulate actin cytoskeleton rearrangements, coordinating cellular movements during epithelial morphogenesis (60). Taken together, our results are consistent with a model whereby high P-Rex1 expression in mammary epithelial cells promotes loss of apicobasal polarity leading to initiation of mammary duct tubulogenesis as a consequence of sustained hyperactivation of Rac1/ERK1/2 signaling and enhanced cell migration.

A significant finding of our study is the demonstration that P-Rex1 expression increases tumor incidence and metastasis, but not tumor growth, cooperating with other oncogenes such as neu. This contrasts with mouse models of melanoma where *Prex1* ablation did not affect primary tumor incidence, latency, or burden (21). P-Rex1 oncogenic effects may be breast cancer subtype specific and/or governed by the microenvironment and/or level of P-Rex1 expression. High *PREX1* transgene expression was required for de novo tumor development; however, the level of transgene expression was less critical in the presence of another oncogene such as neu where both high and low level *PREX1* transgene expression enhanced tumor incidence, initiation, and tumor cell invasion. In an oncogene-driven context the level of P-Rex1 expression may only need to surpass a threshold

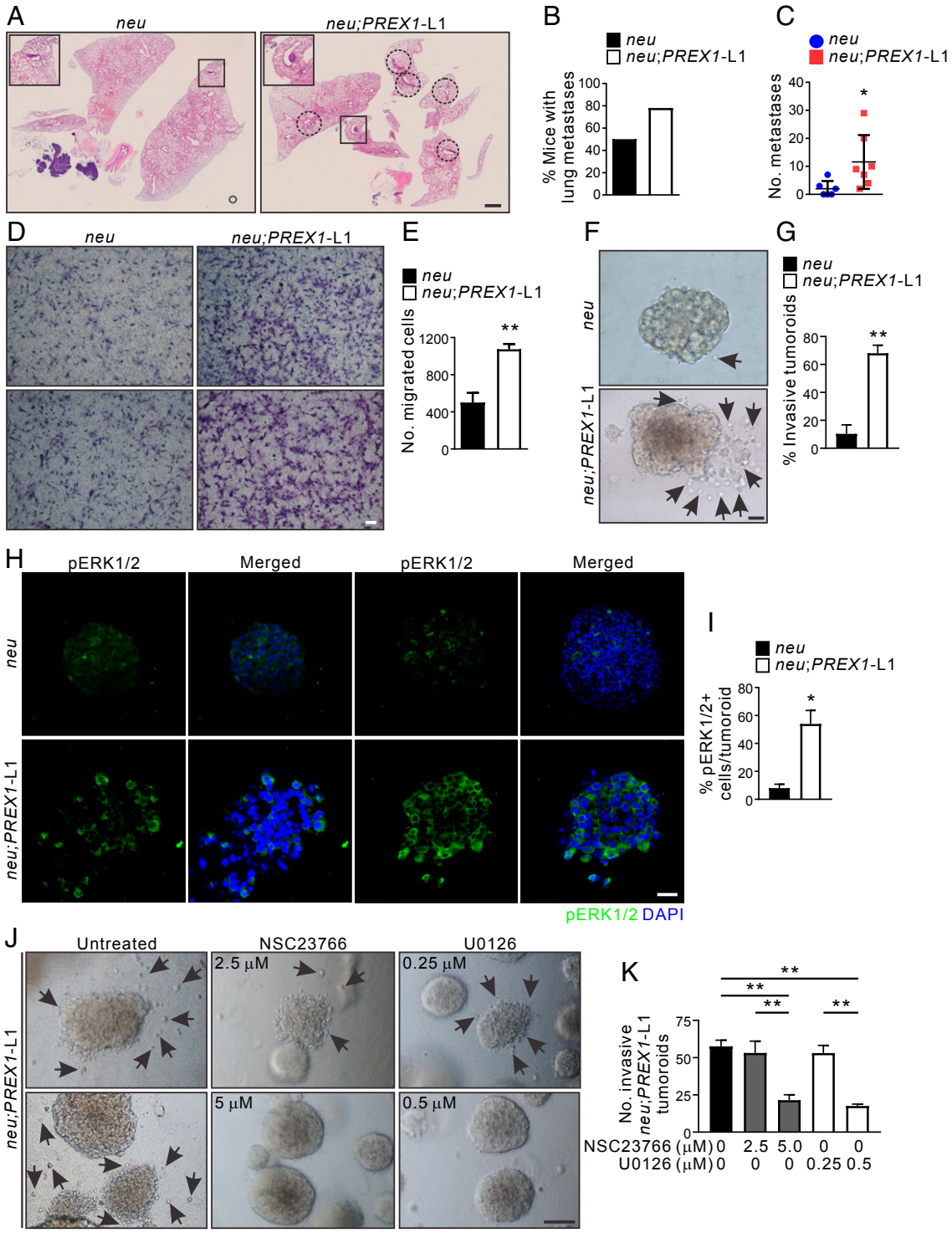

Fig. 7. P-Rex1 overexpression enhances lung metastasis in a *neu*-driven mouse model of breast cancer. (*A*) Formalin-fixed, paraffin-embedded (FFPE) lung sections from MMTV-*neu* and MMTV-*neu;PREX1*^{L1} mice were stained with H&E to identify lung metastases (circled). Higher magnification images of the boxed regions are shown. (*B*) Lung sections from MMTV-*neu* ($n = 6$) and MMTV-*neu;PREX1*^{L1} ($n = 7$) mice were scored for metastases. Data represent the percentage of mice exhibiting lung metastases. (*C*) Quantitation of the number of lung metastases in MMTV-*neu* and MMTV-*neu;PREX1*^{L1} mice. Data represent the mean number of metastases from five lung sections/mouse ± SEM ($n = 6$ to 7 mice, Student's *t* test). (*D* and *E*) Epithelial tumor cell lines were established from mammary tumors from MMTV-*neu* and MMTV-*neu;PREX1*^{L1} mice. Cell migration toward a serum gradient was determined using Transwell assays (*D*). Data represent mean ± SEM ($n = 3$ cell lines/genotype, Student's *t* test) (*E*). (*F* and *G*) Mammary tumoroids from MMTV-*neu* and MMTV-*neu;PREX1*^{L1} transgenic mice were cultured in collagen for 21 d and imaged by brightfield microscopy; arrows indicate invading cells (*F*). Data represent mean invasive tumoroids ± SEM ($n = 3$ mice/genotype, >44 tumoroids/genotype; Student's *t* test) (*G*). (*H* and *I*) FFPE sections of MMTV-*neu* and MMTV-*neu;PREX1*^{L1} mouse mammary tumoroids cultured in collagen 1 were immunostained with a pERK1/2 antibody and DAPI (*H*). Data represent mean pERK1/2-positive cells/tumoroid ± SEM ($n = 3$ mice/genotype, 5 to 15 tumoroids/mouse; Student's *t* test) (*I*). (*J* and *K*) Mammary tumoroids from MMTV-*neu;PREX1*^{L1} transgenic mice were cultured in collagen ± 5 μM NSC23766 or 0.5 μM U0126 for 21 d (*J*). Data represent mean invasive tumoroids ± SEM ($n = 3$ mice/genotype, >127 tumoroids/genotype, one-way ANOVA and Tukey's multiple comparisons test) (*K*). (Scale bars: 2 mm in *A*, 100 μm in *D*, *F*, and *H*, and 50 μm in *J*.) *$P < 0.05$, **$P < 0.01$.

which could account for the lack of phenotypic difference between MMTV-*neu;PREX1*^{L1} and MMTV-*neu;PREX1*^{L2} mice. P-Rex1's intrinsic oncogenic activity and its enhancement of neu's aggressive phenotype may occur early in disease as suggested by the increased tumor incidence. Consistent with this contention we observed increased mammosphere formation of MMTV-*neu*:*PREX1* tumor cells; however, cell proliferation in established tumoroids or primary mammary tumors was not affected. These results are reminiscent of another Rac-GEF, Tiam1, which also regulates breast cancer initiation and metastasis but not tumor growth (61). Interestingly, the enhanced colony formation and invasion observed in tumoroids derived from MMTV-*neu;PREX1*^{L1} primary mammary tumors was suppressed by pharmacological inhibition of Rac1 and MEK1/2, suggesting that P-Rex1 regulates the Rac-ERK1/2 signaling axis to drive initiation and metastasis. Personalized medicine approaches that target P-Rex1–Rac1 signaling as an adjunct therapy, in combination with standard-of-care treatments, may be an avenue for future therapeutic development to reduce disease progression, which is the leading cause of breast cancer deaths. The PI3Kα inhibitor, alpelisib, in combination with fulvestrant (endocrine therapy), was recently approved for treatment of ER^{+ve}/HER2^{-ve} advanced breast cancers; however, a clinically relevant treatment benefit was observed only in cancers with mutant PI3Kα and all patients eventually relapsed (62). Based on the COMBI-AD trial, a combination of the MEK1/2 inhibitor, trametinib, and the BRAF inhibitor, dabrafenib, has been approved for adjuvant treatment of BRAF mutant melanoma (63, 64); however, trametinib has been reported to have limited efficacy in triple negative breast cancer (65). The ERK1/2 inhibitor, ulixertinib, is in clinical trials for the treatment of advanced/metastatic solid tumors (66). Further studies will be required to evaluate the efficacy of PI3K and MEK/ERK inhibitors for treatment of cancers with high P-Rex1 expression.

Materials and Methods

Generation of MMTV-*PREX1* and MMTV-*neu;PREX1* Mice. Full length human *PREX1* cDNA with an N-terminal Myc tag was cloned into the MMTV-SV40-Bssk vector under the control of the murine mammary tumor virus long terminal repeat (MMTV-LTR) promoter followed by the SV40 intron and polyadenylation sequence. A linearized MMTV-Myc-*PREX1* fragment was microinjected into fertilized mouse oocytes to generate two independent MMTV-*PREX1* transgenic founder lines 1 and 2 (MMTV-*PREX1*^{L1} and ^{L2}). MMTV-*PREX1*^{L1} and MMTV-*PREX1*^{L2} mice were generated on a pure FVB/N background by Monash Gene Recombineering. MMTV-*neu;PREX1* transgenic mice were generated by crossing FVB/N female MMTV-*PREX1* mice with FVB/N male MMTV-*neu* mice originally generated by Guy et al., and referred to as MMTV/unactivated neu transgenic mice (25) (kindly provided by Prof Visvader, WEHI, Parkville, Victoria, Australia). The genotype of mice was verified by PCR analysis of genomic DNA using the following primers: *PREX1* (5′ to 3′): GGCCACGACACCATGAGTTATCGC and GGAGAAGGTGCACACGGCGGCCAC; *neu* (5′ to 3′): GGAAGTACCCGGATGAGGAGGGCATATG- and CGGCTTGTACACAGGGACCTGGCTGCCCGG. All MMTV-*PREX1* and MMTV-*neu*;*PREX1* transgenic mice examined were exclusively heterozygous for the *PREX1* and/or *neu* transgene(s) and nulliparous.

Generation of Rac1-FRET; MMTV-*neu;Prex1*$^{-/-}$ and Rac1-FRET; MMTV-*PyMT;Prex1*$^{-/-}$ Mice. *Prex1* knockout mice (51) were crossed with Rac1-FRET mice (55) and either MMTV-*PyMT* (53) or MMTV-*neu* (25) oncogene-driven mammary carcinoma models. Mice were generated on a mixed background (50% C57/BL6, 50% FVB/N).

Statistical Analysis. Statistical analysis was performed using GraphPad Prism 6.02. Graphs represent mean ± SEM. The sample size (*n*) for all experiments is indicated in the figure legends. Survival curves were assessed by a Log-rank Mantel–Cox test. Experiments involving FLIM-FRET, tumoroid growth in the presence of inhibitors, or comparisons of mice at different ages were assessed by one-way ANOVA with Tukey's multiple comparisons test as indicated in the figure legends. All other *P* values were calculated using a two-tailed, unpaired Student's *t* test.

Study Approval. All animal experiments were approved under project license at the Cancer Research UK Beatson Institute or by the Monash University Animal Ethics Committee (MARP/2012/067, MARP/2015/148, MARP/2012/026).

Data Availability. All study data are included in the article and supporting information.

ACKNOWLEDGMENTS. This study utilized the Monash Micro Imaging Facility and Monash Histology Platform (Monash University). We acknowledge the resources, facilities, and scientific and technical assistance of the Monash Biomedicine Discovery Institute Organoid Program (Victoria, Australia). We thank Professor Jane Visvader for the MMTV-*neu* mice. This work was supported by a National Health and Medical Research Council grant (APP1104614).

1. R. Halaoui *et al*., Progressive polarity loss and luminal collapse disrupt tissue organization in carcinoma. *Genes Dev.* **31**, 1573–1587 (2017).
2. N. A. Mack, M. Georgiou, The interdependence of the Rho GTPases and apicobasal cell polarity. *Small GTPases* **5**, 10 (2014).
3. R. B. Haga, A. J. Ridley, Rho GTPases: Regulation and roles in cancer cell biology. *Small GTPases* **7**, 207–221 (2016).
4. E. Wertheimer *et al*., Rac signaling in breast cancer: A tale of GEFs and GAPs. *Cell. Signal.* **24**, 353–362 (2012).
5. S. P. Ngok, W. H. Lin, P. Z. Anastasiadis, Establishment of epithelial polarity–GEF who's minding the GAP? *J. Cell Sci.* **127**, 3205–3215 (2014).
6. H. C. E. Welch, Regulation and function of P-Rex family Rac-GEFs. *Small GTPases* **6**, 49–70 (2015).
7. N. Srijakotre *et al*., P-Rex1 and P-Rex2 RacGEFs and cancer. *Biochem. Soc. Trans.* **45**, 963–977 (2017).
8. K. Hill *et al*., Regulation of P-Rex1 by phosphatidylinositol (3,4,5)-trisphosphate and Gbetagamma subunits. *J. Biol. Chem.* **280**, 4166–4173 (2005).
9. H. C. E. Welch *et al*., P-Rex1, a PtdIns(3,4,5)P3- and Gbetagamma-regulated guanine-nucleotide exchange factor for Rac. *Cell* **108**, 809–821 (2002).
10. M. S. Sosa *et al*., Identification of the Rac-GEF P-Rex1 as an essential mediator of ErbB signaling in breast cancer. *Mol. Cell* **40**, 877–892 (2010).
11. J. C. Montero, S. Seoane, A. Ocaña, A. Pandiella, P-Rex1 participates in Neuregulin-ErbB signal transduction and its expression correlates with patient outcome in breast cancer. *Oncogene* **30**, 1059–1071 (2011).
12. L. Barrio-Real *et al*., Subtype-specific overexpression of the Rac-GEF P-REX1 in breast cancer is associated with promoter hypomethylation. *Breast Cancer Res.* **16**, 441 (2014).
13. L. M. Dillon *et al*., P-REX1 creates a positive feedback loop to activate growth factor receptor, PI3K/AKT and MEK/ERK signaling in breast cancer. *Oncogene* **34**, 3968–3976 (2015).
14. J. D. Marotti, K. E. Muller, L. J. Tafe, E. Demidenko, T. W. Miller, P-Rex1 expression in invasive breast cancer in relation to receptor status and distant metastatic site. *Int. J. Breast Cancer* **2017**, 4537532 (2017).
15. G. Korkmaz *et al*., A CRISPR-Cas9 screen identifies essential CTCF anchor sites for estrogen receptor-driven breast cancer cell proliferation. *Nucleic Acids Res.* **47**, 9557–9572 (2019).
16. W.-Y. Cheng, T. H. Ou Yang, D. Anastassiou, Development of a prognostic model for breast cancer survival in an open challenge environment. *Sci. Transl. Med.* **5**, 181ra50 (2013).
17. Y. Zhong *et al*., Phosphatidylinositol-3,4,5-trisphosphate dependent Rac Exchange Factor 1 (PREX1) is a novel predictor of prognosis for breast cancer patients: A retrospective case series. *Med. Sci. Monit.* **25**, 6554–6562 (2019).
18. H. J. Liu *et al*., PREX1 Rac-GEF activity promotes breast cancer cell proliferation and tumor growth via activation of Extracellular-Signal-Regulated Kinase 1/2 (ERK1/2) Signaling. *J. Biol. Chem.* **291**, 17258–17270 (2016).
19. M. E. Clements, R. W. Johnson, PREX1 drives spontaneous bone dissemination of ER+ breast cancer cells. *Oncogene* **39**, 1318–1334 (2020).
20. L. Barrio-Real *et al*., P-Rex1 is dispensable for Erk activation and mitogenesis in breast cancer. *Oncotarget* **9**, 28612–28624 (2018).
21. C. R. Lindsay *et al*., P-Rex1 is required for efficient melanoblast migration and melanoma metastasis. *Nat. Commun.* **2**, 555 (2011).
22. B. Pereira *et al*., The somatic mutation profiles of 2,433 breast cancers refines their genomic and transcriptomic landscapes. *Nat. Commun.* **7**, 11479 (2016).
23. S. M. Mense *et al*., PTEN inhibits PREX2-catalyzed activation of RAC1 to restrain tumor cell invasion. *Sci. Signal.* **8**, ra32 (2015).
24. B. Fine *et al*., Activation of the PI3K pathway in cancer through inhibition of PTEN by exchange factor P-REX2a. *Science* **325**, 1261–1265 (2009).
25. C. T. Guy *et al*., Expression of the neu protooncogene in the mammary epithelium of transgenic mice induces metastatic disease. *Proc. Natl. Acad. Sci. U.S.A.* **89**, 10578–10582 (1992).
26. A. Tsubura, K. Yoshizawa, N. Uehara, T. Yuri, Y. Matsuoka, Multistep mouse mammary tumorigenesis through pre-neoplasia to neoplasia and acquisition of metastatic potential. *Med. Mol. Morphol.* **40**, 9–17 (2007).
27. A. Raafat *et al*., Effects of age and parity on mammary gland lesions and progenitor cells in the FVB/N-RC mice. *PLoS One* **7**, e43624 (2012).

28. H. Ebi *et al*., PI3K regulates MEK/ERK signaling in breast cancer via the Rac-GEF, P-Rex1. *Proc. Natl. Acad. Sci. U.S.A.* **110**, 21124–21129 (2013).
29. A. B. Hanker *et al*., Mutant PIK3CA accelerates HER2-driven transgenic mammary tumors and induces resistance to combinations of anti-HER2 therapies. *Proc. Natl. Acad. Sci. U.S.A.* **110**, 14372–14377 (2013).
30. J. J. Campbell, C. J. Watson, Three-dimensional culture models of mammary gland. *Organogenesis* **5**, 43–49 (2009).
31. J. Roignot, X. Peng, K. Mostov, Polarity in mammalian epithelial morphogenesis. *Cold Spring Harb. Perspect. Biol.* **5**, a013789 (2013).
32. C. Rejon, M. Al-Masri, L. McCaffrey, Cell polarity proteins in breast cancer progression. *J. Cell. Biochem.* **117**, 2215–2223 (2016).
33. L. Huang, S. K. Muthuswamy, Polarity protein alterations in carcinoma: A focus on emerging roles for polarity regulators. *Curr. Opin. Genet. Dev.* **20**, 41–50 (2010).
34. S. McNally, F. Martin, Molecular regulators of pubertal mammary gland development. *Ann. Med.* **43**, 212–234 (2011).
35. J. L. Inman, C. Robertson, J. D. Mott, M. J. Bissell, Mammary gland development: Cell fate specification, stem cells and the microenvironment. *Development* **142**, 1028–1042 (2015).
36. R. J. Huebner, N. M. Neumann, A. J. Ewald, Mammary epithelial tubes elongate through MAPK-dependent coordination of cell migration. *Development* **143**, 983–993 (2016).
37. G. Li *et al*., Conditional loss of PTEN leads to precocious development and neoplasia in the mammary gland. *Development* **129**, 4159–4170 (2002).
38. K. V. Nguyen-Ngoc, A. J. Ewald, Mammary ductal elongation and myoepithelial migration are regulated by the composition of the extracellular matrix. *J. Microsc.* **251**, 212–223 (2013).
39. D. R. Pitelka, S. T. Hamamoto, J. G. Duafala, M. K. Nemanic, Cell contacts in the mouse mammary gland. I. Normal gland in postnatal development and the secretory cycle. *J. Cell Biol.* **56**, 797–818 (1973).
40. G. Chandramouly, P. C. Abad, D. W. Knowles, S. A. Lelièvre, The control of tissue architecture over nuclear organization is crucial for epithelial cell fate. *J. Cell Sci.* **120**, 1596–1606 (2007).
41. N. J. Godde *et al*., Scribble modulates the MAPK/Fra1 pathway to disrupt luminal and ductal integrity and suppress tumour formation in the mammary gland. *PLoS Genet.* **10**, e1004323 (2014).
42. V. M. Braga, L. M. Machesky, A. Hall, N. A. Hotchin, The small GTPases Rho and Rac are required for the establishment of cadherin-dependent cell-cell contacts. *J. Cell Biol.* **137**, 1421–1431 (1997).
43. Y. S. Chu *et al*., Force measurements in E-cadherin-mediated cell doublets reveal rapid adhesion strengthened by actin cytoskeleton remodeling through Rac and Cdc42. *J. Cell Biol.* **167**, 1183–1194 (2004).
44. A. Kraemer, M. Goodwin, S. Verma, A. S. Yap, R. G. Ali, Rac is a dominant regulator of cadherin-directed actin assembly that is activated by adhesive ligation independently of Tiam1. *Am. J. Physiol. Cell Physiol.* **292**, C1061–C1069 (2007).
45. C. Albanese *et al*., Transforming p21ras mutants and c-Ets-2 activate the cyclin D1 promoter through distinguishable regions. *J. Biol. Chem.* **270**, 23589–23597 (1995).
46. J. N. Lavoie, G. L'Allemain, A. Brunet, R. Müller, J. Pouysségur, Cyclin D1 expression is regulated positively by the p42/p44MAPK and negatively by the p38/HOGMAPK pathway. *J. Biol. Chem.* **271**, 20608–20616 (1996).
47. R. Montesano *et al*., Differential effects of hepatocyte growth factor isoforms on epithelial and endothelial tubulogenesis. *Cell Growth Differ.* **9**, 355–365 (1998).
48. L. E. O'Brien *et al*., ERK and MMPs sequentially regulate distinct stages of epithelial tubule development. *Dev. Cell* **7**, 21–32 (2004).
49. D. J. Eastburn, M. M. Zegers, K. E. Mostov, Scrib regulates HGF-mediated epithelial morphogenesis and is stabilized by Sgt1-HSP90. *J. Cell Sci.* **125**, 4147–4157 (2012).
50. L. E. Dow *et al*., The tumour-suppressor scribble dictates cell polarity during directed epithelial migration: Regulation of Rho GTPase recruitment to the leading edge. *Oncogene* **26**, 2272–2282 (2007).
51. H. C. Welch *et al*., P-Rex1 regulates neutrophil function. *Curr. Biol.* **15**, 1867–1873 (2005).
52. A. Fantozzi, G. Christofori, Mouse models of breast cancer metastasis. *Breast Cancer Res.* **8**, 212 (2006).
53. C. T. Guy, R. D. Cardiff, W. J. Muller, Induction of mammary tumors by expression of polyomavirus middle T oncogene: A transgenic mouse model for metastatic disease. *Mol. Cell. Biol.* **12**, 954–961 (1992).
54. E. Y. Lin *et al*., Progression to malignancy in the polyoma middle T oncoprotein mouse breast cancer model provides a reliable model for human diseases. *Am. J. Pathol.* **163**, 2113–2126 (2003).
55. A. E. Johnsson *et al*., The Rac-FRET mouse reveals tight spatiotemporal control of Rac activity in primary cells and tissues. *Cell Rep.* **6**, 1153–1164 (2014).
56. J. Qin *et al*., Upregulation of PIP3-dependent Rac exchanger 1 (P-Rex1) promotes prostate cancer metastasis. *Oncogene* **28**, 1853–1863 (2009).
57. J. E. Fata *et al*., The MAPK(ERK-1,2) pathway integrates distinct and antagonistic signals from TGFalpha and FGF7 in morphogenesis of mouse mammary epithelium. *Dev. Biol.* **306**, 193–207 (2007).
58. W. Zhu, C. M. Nelson, PI3K regulates branch initiation and extension of cultured mammary epithelia via Akt and Rac1 respectively. *Dev. Biol.* **379**, 235–245 (2013).
59. A. J. Ewald *et al*., Mammary collective cell migration involves transient loss of epithelial features and individual cell migration within the epithelium. *J. Cell Sci.* **125**, 2638–2654 (2012).
60. A. Ivetic, A. J. Ridley, Ezrin/radixin/moesin proteins and Rho GTPase signalling in leucocytes. *Immunology* **112**, 165–176 (2004).
61. K. Strumane, T. Rygiel, M. van der Valk, J. G. Collard, Tiam1-deficiency impairs mammary tumor formation in MMTV-c-neu but not in MMTV-c-myc mice. *J. Cancer Res. Clin. Oncol.* **135**, 69–80 (2009).
62. F. André *et al*.; SOLAR-1 Study Group, Alpelisib for PIK3CA-mutated, hormone receptor–positive advanced breast cancer. *N. Engl. J. Med.* **380**, 1929–1940 (2019).
63. G. V. Long *et al*., Adjuvant Dabrafenib plus Trametinib in stage III BRAF-mutated melanoma. *N. Engl. J. Med.* **377**, 1813–1823 (2017).
64. R. Dummer *et al*., Adjuvant dabrafenib plus trametinib versus placebo in patients with resected, $BRAF^{V600}$-mutant, stage III melanoma (COMBI-AD): Exploratory biomarker analyses from a randomised, phase 3 trial. *Lancet Oncol.* **21**, 358–372 (2020).
65. B. Ramaswamy *et al*., Abstract LB-216: NCI 9455: Phase II study of trametinib followed by trametinib plus AKT inhibitor,GSK2141795 in patients with advanced triple negative breast cancer. *Cancer Res.* **76**, LB-216 (2016).
66. R. J. Sullivan *et al*., First-in-class ERK1/2 inhibitor Ulixertinib (BVD-523) in patients with MAPK mutant advanced solid tumors: Results of a phase I dose-escalation and expansion Study. *Cancer Discov.* **8**, 184–195 (2018).